On the Design of an Autonomous Robot Fish

Dimitrios Tzeranis[1], Evangelos Papadopoulos[1], *Senior Member*, *IEEE*, and George Triantafyllou[2]

***Abstract*—A fish-like propulsion system seems to be an interesting and efficient alternative to propellers in small underwater vehicles. This paper presents the early design stages of a small autonomous robotic vehicle driven by an oscillating foil. It describes the preliminary dimensioning of the vehicle and the selection and sizing of the necessary actuators according to the project's objectives and constraints. Finally there is a description of the control system implementation for the tail's motion.**

***Index terms*—Fish propulsion, underwater robot, fish design.**

I. Introduction

ALTHOUGH almost all marine vehicles use propellers for their propulsion, propellers and especially those designed for small underwater vehicles are not very efficient, their efficiency being no more than 40 percent, [1]. The main cause is the production of vortices perpendicular to the direction of motion. Due to their orientation, these vortices do not produce thrust, though they increase power consumption.

An alternative apparatus for thrust development is the oscillating foil. The production of thrust is based in the formation of a reverse Karman vortex street in the flow wake. Thrust generation and its sensitivity to the Strouhal number is similar to the efficient propulsion of fish.

The implementation of a fish-like propulsion mechanism is not possible in ships and submarines due to practical constraints. However its use in small underwater vehicles is promising and motivated many previous studies. The most famous one is MIT's Robotuna, which was used to study fish propulsion mechanisms, [1, 2]. Berkeley's Calibot, various projects at Japan's NMRI and Draper's VCUUV are examples of autonomous fish robots, [3, 4, 5].

In this work, an underwater vehicle is developed, characterized by (a) an efficient oscillating foil propulsion mechanism, (b) power autonomy for at least one hour, (c) the ability to move across rectilinear or curviform paths (two dimensional motion), (d) low cost so that the possibility of losing does not make its use prohibitive, (e) the presence of a visual sensor allowing use in inspection tasks. This paper discusses design and implementation issues related to the development of this vehicle.

[1] Control Systems Laboratory, Department of Mechanical Engineering, National Technical University of Athens, 157 80 Athens, Greece, (e-mail: egpapado@central.ntua.gr).
[2] Department of Naval Architecture, National Technical University of Athens, 157 80 Athens, Greece.

II. Thrust Development In Oscillating Foils And Application in Underwater Vehicles

A marine vehicle, moving at velocity $\overline{u}_{i.a}$ with respect to the immobile water, can produce thrust by creating a water jet of mass flow $\dot{m}$ along the direction of its motion. If the water jet's average relative velocity with respect to the vehicle is $\overline{u}_{o.a}$, then the average thrust force F equals to

$$F = \dot{m}(\overline{u}_{o.a} - \overline{u}_{i.a}) \quad (1)$$

One method for creating a jet is through an oscillating foil that generates a reverse Karman vortex street in the wake of the flow, [6]. This phenomenon is independent of the Reynolds number but depends strongly on the nondimensional Strouhal number:

$$St = f \cdot d / U \quad (2)$$

where f is the frequency of the foil's oscillation, d is the width of the wake and $U = \overline{u}_{i.a}$. The Strouhal number must lie between 0.25 and 0.35 in order to produce thrust, otherwise the oscillating foil induces drag, [6]. According to fish observations, the width d is assumed to be a constant. Therefore, keeping the St in the above range for various vehicle speeds is accomplished by varying frequency f. This means that f becomes a function of U.

The influence of Strouhal number in "tuning" an oscillating foil to produce thrust is also observed in fish using the carangiform swimming mode. Those fish produce thrust by undulary motions of the rear part of their body and their tail. The Strouhal number in this case also lies between 0.25 and 0.35 [6].

It would have been impossible for fish to use conventional propulsive mechanisms, because they do not possess the necessary muscle power to propel themselves in the observed velocities (Gray's paradox [7]). This is an indication that fish swimming reduces drag through advanced hydrodynamic mechanisms. Specifically fish reduce their drag in two ways [2]: (a) The undulatory body motion delays the transition of the boundary layer from laminar into turbulent and the separation of the flow. (b) While the motion of a rigid body inside water induces drag due to flow separation and creation of a Karman vortex street in the wake, fish sense the position of those vortices and use their tail to change vortex trajectories (vortex control). In this way they produce a thrust-creating reverse Karman vortex street, see Fig. 1.

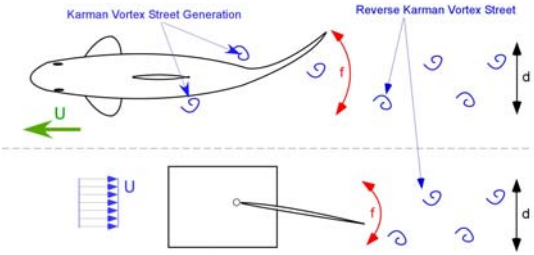

Figure 1. Analogy in thrust generation between a swimming fish and an oscillating foil apparatus.

Fish swimming is classified as *carangiform*, *anguiliform*, *thunninform* and *ostraciform*, depending on the percentage of their body that contributes in thrust production through undulatory motions. According to this observation, there are three alternative ways to design a robot fish, see Fig. 2,

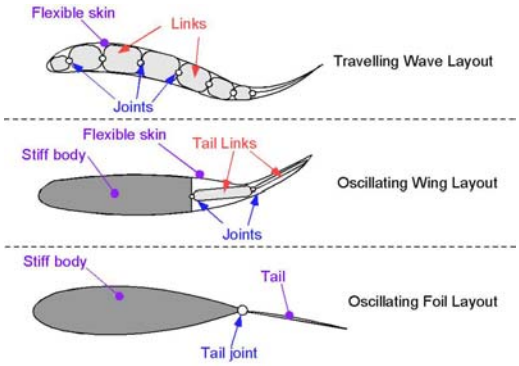

Figure 2. Alternative ways for robot fish design.

(a) The "traveling wave" design. Thrust is generated by undulatory motions that travel through the whole body, with amplitude that increases backwards. This style allows the design of extremely small robots using Shape Memory Alloy (SMA) wires, [8]. However the poor efficiency of SMAs precludes the design of a system with a useful range. This style is dropped due to the many required joints that complicate the design and increase friction losses.

(b) The "oscillating wing" design. Thrust is generated by undulatory motions of the rear and of the tail. Many variations of this design exist, which depend on the contribution of the body in thrust generation. The amount of thrust provided at various speeds and the hydraodynamic efficiency varies with the design. This design imitates the most efficient swimming modes of fish, however it is still quite complex for small vehicles.

(c) The "oscillating plate" design. The body of the fish robot is rigid while thrust is generated by an oscillating tail connected to the body through a joint. This design style has the worse hydrodynamic performance because of the rigid body. However it provides the simplest design: less joints, less mechanical losses due to friction, simple and inexpensive construction, simple control and finally less weight. For these reasons, this is the design employed.

III. Actuator Selection

The motion of the tail can be described by the equation,

$$\theta(t) = \theta_\alpha + \theta_0 \cdot \cos(2\pi f t) \quad (3)$$

where $\theta(t)$ is the angle between the tail and the longitudinal axis of the vehicle, θ_α is the mean of θ during one period and f is the frequency of the oscillating foil. The tail's motion system must be able to vary the parameters of motion f, θ_α και θ_0 for the following reasons.

First, as explained earlier, the tail frequency f must be a function of U so as to keep the Strouhal number in the optimum range [0.25, 0.35]. Although this range is theoretically derived for a constant U, it is assumed that it is also valid during turning and accelerating. In the case of vehicle body length L≤25 cm and speed U≤ 30 cm/s then f≤ 3 Hz.

Changing θ_α allows for turning and maneuvering. The axis of the mean thrust force F forms an angle θ_α with the longitudinal vehicle axis and passes through the tail joint, see Fig. 3. The mean torque generated by F and applied to the vehicle's center of mass G_v is

$$T = F \cdot L_J \cdot \sin(\theta_\alpha) \quad (4)$$

where L_J is the distance between the center of mass G_v and the tail's joint across the longitudinal axis of the vehicle. When $\theta_\alpha \neq 0$ the vehicle turns due to the mean torque T.

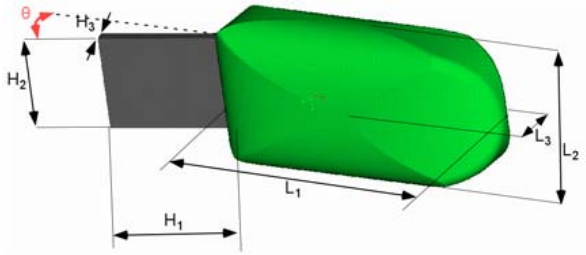

Figure 3. Basic mechatronic fish geometry.

Note that another way for turning is by commanding the tail at a large angle θ. In this case, the hydrodynamic drag exerted on the tail produces a torque that changes the orientation of the vehicle. Still, the ability to control the mean tail angle θ_a is needed.

The amplitude of a tail's motion θ_0 is assumed to be constant and independent of the vehicle's speed U when this speed is constant This assumption is based on observations of fish swimming kinematics, [6]. Being able to vary θ_0 increases the maneuvering ability of the vehicle.

The selection of the proper actuator is based not only on the characteristics of the various actuator technologies, [9] but also on the various actuator designs that are able to realize a tail motion system capable of varying the motion parameters f, θ_α and θ_0. The four candidate designs are:

Design 1: Two antagonistic linear actuators. Its drawbacks include the need for a distinct drive for each actuator, the presence of large forces due to actuator preloads and antagonistic design, and fatigue problems (depending on actuator technology used).

Design 2: An actuator and a spring in competition. The drawbacks here include the asymmetry in the system's dynamics, and the demand for an actuator displacement that is double the one in Design 1.

Design 3: An actuator that provides alternating displacements. The actuator's displacement is converted into tail motion by a simple transmission. The disadvantage here is the increase in power consumption due to alternating accelerations and decelerations of actuator inertia.

Design 4: Utilization of three actuators, each controlling one of the f, θ_α and θ_0. Here, the rotary motion of a motor is converted into an oscillating tail motion by a cam–like mechanism. The motor speed is proportional to the tail's motion frequency *f*. The other two actuators vary θ_α and θ_0 by altering mechanism kinematic parameters. This actuation system is controlled easily. However, the presence of three actuators and a complex mechanism makes the design complicated, heavy and difficult to waterproof. Therefore this layout is not considered further.

SMA wires have minimal weight, are corrosion resistant and characterized by large force to weight ratio. However, due to their poor efficiency (3%), which constrains the autonomy of a vehicle, their utilization is not favored.

Piezoelectric (PZT) actuators are characterized by reasonable efficiency (50%) and large force to mass ratio. However, strains from PZT are too small, i.e. in the order of μm, and mechanisms needed to amplify these tend to be expensive and difficult to manufacture. Furthermore, in a battery-powered vehicle, it is difficult to provide the necessary voltage range for PZT stack actuators (-10 to +150 V). Therefore, PZTs are not a pertinent choice.

Linear voice coils are simple to control and provide adequate displacements. However, the variety of available products is poor. Simulations showed that the few available actuators were not appropriate for this application, and hence their use was not favored.

The control of a stepper motor shaft's position usually can be accomplished without a position sensor. However, due to the changing characteristics of underwater motion, there is a serious possibility of missing steps. Furthermore, the stepped motion may excite tail vibrations and increase hydrodynamic losses. Finally, for the same nominal power, a stepper motor is usually heavier than a DC motor. For the above reasons, stepper motors were not considered further.

DC permanent magnet motors are simple and commercially available in great variety. They may be purchased in combination with the necessary gear head and encoder in a single block that minimizes weight and simplifies design and control. Their handicaps, i.e. brush wear and electric noise production, are not so important in this application.

Table I shows the suitability of various actuator technologies with respect to candidate tail system designs.

TABLE I
ACTUATOR SUITABILITY FOR CANDIDATE TAIL MOTION SYSTEM DESIGNS.

	Design 1	Design 2	Design 3
SMA	•	•	
PZT Actuators		•	
Voice Coils		•	•
Stepper Motors			•
DC Motors			•

Since SMA wires, PZT actuators and linear voice coils were considered unsuitable for this application, Designs 1 and 2 were dropped. The final choice for the realization of the tail motion system is through a DC motor.

IV. ACTUATOR SIZING

Vehicle Motion Load. The vehicle, see Fig. 3, is divided into the main body (modeled as a three dimensional ellipsoid with length L_1, height L_2 and width L_3) and the tail (modeled as a parallelepiped with length H_1, height H_2 and width H_3 = 3 mm). From real life experience and to simplify the choices, the following dimension ratios were chosen: $L_1 = 2L_2$, $3L_1 = 10L_3$ and $5H_1 = 7H_2$. The ratio $\lambda = L_1/H_1$ is determined later. The mass m_w of the vehicle's body equals the mass of the displaced water and is given by

$$m_w = 78.38 \cdot L_1^3 . \quad (5)$$

In order to estimate quickly the added mass coefficient across the longitudinal axis of the vehicle m_{11}^{am}, the body is modeled as an ellipsoid with large axis of length $L_b = L_1$ and small axis of length $L_s = \sqrt{L_2 \cdot L_3}$ (the width and the height of an ellipsoid equals L_s). Then L_s/L_b=0.41 so using tables in [10, page 147], the added mass is estimated to be equal to

$$m_{11}^{am} = 0.18 \cdot m_w = 14.11 \cdot L_1^3 \quad (6)$$

The total equivalent mass of the vehicle *m* when it is traveling along a straight path is

$$m = 1.1 \cdot (m_w + m_{11}^{am}) \approx 100 \cdot L_1^3 \quad (7)$$

where the 1.1 factor is used as compensation for the uncertain shape of the body. The mean propulsive force *F* necessary for the general motion of the vehicle along a straight path equals the sum of the inertial force $F_{inertial}$ (due to the equivalent mass m) and the hydrodynamic drag F_{hydro}

$$F_{inertial} = (m_w + m^{am}) \cdot \dot{U} \approx 100 \cdot L_1^3 \cdot \dot{U} \quad (8)$$

$$F_{hydro} = 0.5 \cdot \rho_w \cdot c_D \cdot A \cdot U^2 \quad (9)$$

where A is the frontal area of the body. The drag coefficient c_D for spheroids is found in tables ([11], page 419) to be *0.27* for laminar flow and *0.13* for turbulent flow, while a transition occurs at Reynolds number Re = 10^5 ($Re = U \cdot L_1 / \nu$). Assuming $U \le 30$ cm/s and $L_1 \le 25$cm and with the kinematic viscosity of water at 20° C equal to $\nu = 10^{-6}$ m^2/s, the maximum expected Reynolds number of the flow is Re=$7.5 \cdot 10^4$. Therefore, the flow around the vehicle is expected to be laminar and c_D = 0.27. Then, the drag and the power it dissipates are given by

$$F_{hydro} \approx 16 \cdot L_1^2 \cdot U^2 \ , \ P_{hydro} \approx 16 \cdot L_1^2 \cdot U^3 \quad (10)$$

Tail Motion Load. The equivalent inertia of the tail I_{zz} with respect to the tail's joint axis equals the sum of the mass inertia of the tail I_{zz}^m and the inertia of the accelerated water I_{zz}^{am}. The later is calculated through the corresponding added mass coefficient,

$$I_{zz}^{am} = \int_0^{H_1} y^2 \cdot \rho_w \cdot \pi / 2 \cdot \left(2 \cdot (H_2/2)^2 + b^2\right) dy \approx 125 \cdot H_1^5 \quad (11)$$

$$I_{zz}^{m} = \rho_f H_1 H_2 H_3 (4H_1^2 + H_3^2) \big/ 12 \approx 1.1 \cdot H_1^4 \quad (12)$$

In order to calculate the damping torque, caused by hydrodynamic drag on the tail, the tail is segmented into segments of length H_2 and width dr, where r is the radial direction, parallel to the length H_1 of the tail. The elementary hydrodynamic drag force that is exerted on each segment can be approximated as

$$dF_{damp} = 0.5 \cdot \rho_w \cdot c_{Dt} \cdot H_2 \cdot dr \cdot u^2 \quad (13)$$

where $u = \omega_L \cdot r$. As a rough approximation, it is assumed that the tail is perpendicular to the flow and therefore the drag coefficient is $c_{Dt} = 2$. The elementary torque with respect to the tail's joint axis dT_{damp} generated by dF_{damp} is $dT_{damp} = r \cdot dF_{damp}$. Integrating the elementary torques along the radial direction provides the total damping torque:

$$T_{damp} = \frac{1}{2} \cdot \rho_w \cdot c_{Dt} \cdot \frac{5}{7} \cdot H_1 \cdot \int_0^{H_1} r^3 dr\, \omega_L^2 = 175 \cdot H_1^5 \cdot \omega_L \cdot |\omega_L| \quad (14)$$

The total torque needed for the motion of the tail is:

$$T_L = 175 H_1^5 \omega_L |\omega_L| + 1.1 H_1^4 \dot{\omega}_L + 125 H_1^5 \dot{\omega}_L \quad (15)$$

The first term in Eq. (15) represents the damping torque due to hydrodynamic drag, the second term represents the torque that accelerates the inertia of the tail and the third term represents the torque that accelerates water due to tail motion. Only the third term contributes in thrust production (the "useful" part of T_L). Therefore the total power consumption for the tail motion $P_L = T_L \cdot \omega_L$ is divided into a "useful" P_{L_use} and a "waste" part P_{L_waste}.

$$P_{L\_use} = 125 \cdot H_1^5 \cdot \dot{\omega}_L \cdot \omega_L \quad (16a)$$

$$P_{L\_waste} = 175 \cdot H_1^5 \cdot \omega_L^2 \cdot |\omega_L| + 1.1 \cdot H_1^4 \cdot \dot{\omega}_L \cdot \omega_L \quad (16b)$$

For the case of sinusoidal tail motion $\theta = \theta_0 \cdot \cos(2\pi f t)$, the integration of the "useful" power P_{L_use} over one period of motion $T=1/f$ provides the average "useful" power (the average power that is used in accelerating water)

$$\overline{P}_{L\_use} = \frac{4}{T} \int_0^{T/4} P_{L\_use}(t) dt = 1000 \cdot f^3 \cdot \pi^2 \cdot H_1^5 \cdot \theta_0^2 \quad (17)$$

The average propulsive power can be computed using the oscillating tail hydrodynamic efficiency η_h, i.e. the percentage of the power used for water acceleration that transforms into propulsive power. Assuming that $\eta_h \approx 0.7$ (efficiencies higher than 85% have been reported [4]), then

$$P_{prop} = \eta_h \cdot \overline{P}_{L\_use} = \eta_h \cdot 1000 \cdot f^3 \cdot \pi^2 \cdot H_1^5 \cdot \theta_0^2 \quad (18)$$

Constant Speed Motion. The width of the wake that is created by an oscillating foil is approximated by [6]

$$d \approx 2 \cdot H_1 \cdot \sin(\theta_0) \quad (19)$$

Using the Strouhal constraint, assuming that the tail motion frequency f is a function of U and substituting the result in Eq. (18), the average propulsive power becomes

$$P_{prop} = 125 \cdot \eta_h \cdot \pi^2 \cdot St^3 \cdot H_1^2 \cdot \theta_0^2 \cdot U^3 \big/ \sin(\theta_0)^3 \quad (20)$$

When the vehicle's speed U is constant, the power dissipation due to hydrodynamic drag, P_{hydro}, equals the average propulsive power P_{prop}. Using Eqs. (10)-(20), the ratio λ for the vehicle to travel with constant U is:

$$\lambda = \frac{L_1}{H_1} = \frac{5 \cdot \pi}{4} \cdot \sqrt{\frac{5 \cdot St^3 \cdot \eta_h \cdot \theta_0^2}{\sin(\theta_0)^3}} \quad (21)$$

According to Eq. (21), for a given body of length L_1, the tail's length H_1 is a function of the tail's Strouhal number (for constant η_h, θ_0). Eq. (21) provides an estimation of the tails's length H_1 range that corresponds to the optimum Strouhal range. This tail length range is useful in order to size the necessary actuators.

Primary Sizing for the Vehicle. Functional, economic and production constraints play a role in minimizing the size of the vehicle. A lower bound exists in the weight of the vehicle due to the weight of the included components (actuator, battery, electronics, sensor). According to the first estimation of the body's shape, its weight lies between 320g (L_1=16cm) and 1200g (L_1=25cm). The weight of the battery (the heaviest component) is about 100g while the weight of electronic circuit boards will be less than 100g. Therefore a reasonable body length is L_1=20cm (the weight in this case is about 620g). The power dissipation due to hydrodynamic losses at constant speed U in the range 10 to 25 cm/s is estimated to be between 1 and 16 mW.

Production constraints include the availability of appropriate production equipment and the fact that cost increases when the vehicle's dimensions become exceedingly small. Judging by the up to now selection of electronic elements and the capabilities of our machine-shop, it seems that a length of L_1 = 20cm is large enough so that the necessary components are commercially available in reasonable prices whereas the structural parts of the vehicle can be manufactured in ordinary machine tools.

The amplitude θ_0 of the tail's motion (case of constant speed U) should not be excessively large in order to prevent flow separation. In this case, oscillating foil thrust production is doubtful. The reasonable estimation $\theta_0 = 15^o$ is based on observations of fish swimming kinematics, [6]. For $\theta_0 = 15^o$ and St = 0.3, Eq. (21) gives $\lambda = 2.4$ and the corresponding tail length is $H_1 = L_1/\lambda = 8.33$cm.

DC Motor Sizing. The "useful" T_{L_use} and the "waste" part T_{L_waste} of the total torque T_L needed for the tail's motion are easily derived from the corresponding power P_{L_use} and P_{L_waste}. Fig. 4 presents calculations of T_{L_use}, T_{L_waste} and T_L for the first vehicle sizing ($\theta_0=15^o$, $L_1 = 20$ cm and $H_1 = 8.3$ cm) in the case of sinusoidal tail motion $\theta=\theta_0 \cdot \cos(2\pi f t)$. It is shown that T_{L_use}, T_{L_waste}, (which is dominated by hydrodynamic losses) and T_L are sinusoidal functions of a common frequency f(U). Their amplitude is $|T_{L\_use}|$ = 22 mN·m, $|T_{L\_waste}|$ = 7 mN·m and $|T_L|$ = 25 mN·m, respectively. Due to 90° phase lag between T_{L_use} and T_{L_waste}, the difference $|T_L|-|T_{L\_use}|$ is smaller than $|T_{L\_waste}|$. The ratio $|T_{L\_use}|/|T_L|$=0.88 (likely to increase due to the

overestimation of the hydrodynamic losses) is an indication of the mechanical part η_m of the tail's total efficiency η_{tail}.

$$\eta_p = \eta_m \cdot \eta_h \tag{22}$$

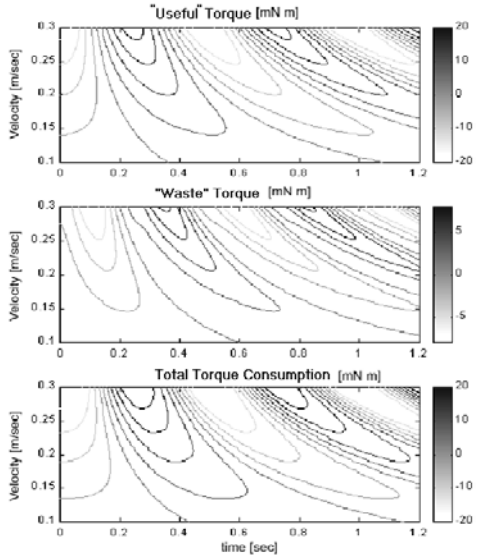

Figure 4: "Useful", "waste" and total torque computation (H_1 = 8.3 cm, θ_0 = 15°).

The angular speed of the tail is a sinusoidal function of time, its amplitude is 22 rpm when *U=20* cm/s and 33 rpm when U = 30 cm/s. The calculations presented in Fig. 4 are valid in the case of tail length H_1 = 8.3cm, which is calculated by Eq. (21) when St=0.3. For each value of tail length H_1 inside the expected range (that results from Eq. (21) for $\mathrm{St} \in [0.25, 0.35]$) there are different results in the calculations of tail's angular velocity ω_L and necessary torque T_L. For a given constant velocity U (constant P_{hydrp}) and assuming constant η_h the average "useful" power $\overline{P}_{L\_use} = P_{hydro} / \eta_h = \int_0^{1/f} T_{L\_use} \cdot \omega_L \cdot dt$ remains unchanged. Therefore a reduction of the Strouhal number induces a reduction in the tail's angular speed, a larger tail (Eq. (21)) and larger necessary torque T_L. In the case of constant U and η_h the average consuming power $\overline{P_L}$ remains almost constant and independent of the Strouhal value.

The dc motor selection is guided by two operating points (ω_L,T_L). The first one is the "design point" of the vehicle, where the tail load is calculated for constant vehicle speed U = 20 cm/s. The second one is the "maximal operating condition", where the tail load is calculated for constant *U*=30 cm/s. Torque T_L and angular speed ω_L at these points equal the maximum expected values of T_L and ω_L. The late correspond to the tail lengths H_1 that are calculated by Eq. (21) when *St* = 0.25 and *St* = 0.35 respectively. Results are shown in Table II.

TABLE 2:
THE OPERATING POINTS CONSIDERED FOR MOTOR SELECTION.

Operating point	ω_L [rpm]	T_L [mN·m]
Design point	32	17
Maximal operating point	48	38

During the motor selection and sizing, it is considered that the transmission system between the output of the motor's gear head and the tail has a mechanical efficiency of 75% and a reduction ratio equal to unity.

An appropriate selection for the DC motor would have low weight (below 40g) and be able to provide the necessary torque and angular speed, displayed in Table 2, with adequate margins. Furthermore it is desired that the motor, a gear head of proper reduction ratio and the necessary encoder are integrated into a single unit.

The DC motor that satisfies the requirements is the RE10 from Maxon Motors (1500 mW maximum power). The motor's nominal voltage is chosen 6 V in order to be supplied efficiently by a battery pack of a few cells. The motor is accompanied by a GP10K gear head (reduction ratio 64:1 and maximum efficiency 70%) and a Digital MR encoder (16 pulses/turn, 2 channels) in a single unit of 10 mm diameter, 48.4 mm length and 17g weight.

The determination of the required motor driver capabilities (voltage and current supply range) is accomplished through simulation on a simple closed loop model. The plant's model consists of the motor (resistance R and inductance L of its windings, and torque constant K_T), the tail (hydrodynamic drag and equivalent inertia I_{zz}) and the transmission (efficiency). The system nonlinearities apart from the hydrodynamic drag, and the driver dynamics were neglected while the controller was a simple PD. In the maximal operating point of *U*=30 cm/s, the required voltage and current appear to be sinusoidal functions whose maximum amplitudes are 2.5 V (when *St* = 0.35) and 250 mA (when *St* = 0.25) respectively.

V. CONTROL SYSTEM IMPLEMENTATION

A simple closed loop control system for the position $\theta(t)$ of the tail is adequate in order to get the desired tail motion, as described by Eq. (3). The direct measurement of angle θ would complicate the design. On the other hand the measurement of the motor's shaft position θ_m using the encoder is straightforward and therefore preferred (the relationship between θ and θ_m is linear). As depicted in Fig. 5, the elements that realize the control system are:

(a) A Microchip PIC16F876 microcontroller. This chip implements the discrete control law and calculates the reference angle θ_{mR}. The variation of the tail motion parameters f, θ_α and θ_0 is carried out by the proper generation of θ_{mR}. Finally it generates a PWM control signal for the DC motor driver.

(b) A battery pack of five AAA NiMH cells of 700 mAh capacity. It provides at least one hour power autonomy, provided that the main current drain is due to the tail motion. The battery's nominal voltage is 6 V, close enough to the output of the voltage regulator (5V), in order to maximize its efficiency. Its weight is about 70g.

(c) Two Maxim 500 mA linear voltage regulators MAX603C that provide 5V fixed or an adjustable output by using two external resistors. The first regulator provides the necessary V_{CC} = 5V supply for the integrated circuits of the

vehicle. The second one provides the motor driver IC voltage supply V_{DD}. The use of two voltage regulators aims in isolating the electric noise produced by the motor driver and in the ability of adjusting V_{DD}. The extremely low (below 0.3V) dropout voltage allows the supply from a 5-cell secondary battery. This combination results in a voltage regulator nominal efficiency of 83%.

(d) An Intersil 500mA full bridge MOSFET power driver HIP4020. This IC has built in free-wheeling diodes and over-current limit protection and it is easily interfaced with microcontrollers capable of generating PWM signals.

(e) An Agilent quadrature decoder/counter HCTL2016 that interfaces the encoder signal to the microcontroller, through a 8bit data bus, in order to reduce its computational load. It rejects noise from the encoder signal, quadruplicates the encoder resolution and increases or decreases a 16bit counter depending on the direction of motor's rotation.

Fig. 6 shows the custom-made PCB board and the employed DC gear-motor with its integral encoder.

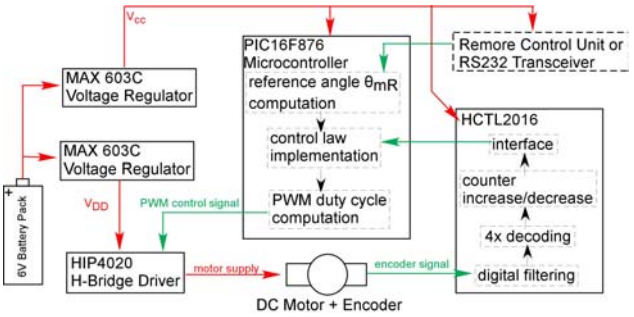

Figure 5. Schematic diagram of the tail motion control system.

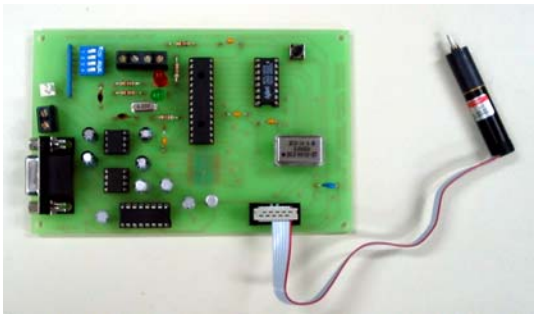

Figure 6. Control system PCB and tail motion 1.5 W micromotor.

The sampling frequency of the control system is estimated in the range of 200 – 400 Hz. The microcontroller needs 30 μsec to read θ_m[k] from the HCTL2016 counter. The reference angle computation θ_{mR}[k] is performed in the previous control loop [k-1] to minimize the delay between reading θ_m[k] and generating the corresponding PWM signal control voltage V[k]. The reference angle θ_{mR}[k] computation is accomplished by discrete sampling of 128 values located in PIC's EEPROM that describe one quarter of a sinusoidal signal. The variation of tail's frequency f is implemented by varying the discrete data sampling period N. The variation of amplitude θ_0 is accomplished by multiplying with an appropriate factor whereas the variation of θ_a is accomplished by adding a desirable angle. Therefore the variation of tail motion parameters f, θ_0 ,θ_a is accomplished through proper θ_{mR}[k] computation. In order to calculate V[k], PIC implements the control law

$$V[k] = a \cdot V[k-1] + b \cdot e[k-1] + c \cdot e[k] \qquad (23)$$

where e[k]= θ_{mR}[k] - θ_m[k]. The calculation of the first two terms is done in the previous control loop. Choosing the discrete controller parameters in Eq. (23), is done either by emulating a continuous PD controller or by discrete state feedback. The main design goal is to achieve a discrete frequency response gain of 0.99 for frequencies up to 30 rad/s. Finally the microcontroller "translates" the value of V[k] into an appropriate PWM duty cycle. The resulting PWM signal together with a direction signal that depends on the sign of V[k] are sent to the motor driver HIP4020.

The user of the vehicle will be able through an RF transceiver to change the velocity or the orientation of the vehicle. At the moment the communication link is implemented by a serial RS232 interface.

VI. Conclusions And Future Work

This paper describes early design choices and sizing of an underwater fish-like vehicle and its actuation subsystem. At the moment our work is concentrated in designing and constructing the vehicle, verifying control laws for the tail motion system and measuring the hydrodynamic characteristics and efficiency of the oscillating foil apparatus.

VII. References

[1] Triantafyllou, M. S. and Triantafyllou, G. S., "An Efficient Swimming Machine", *Scientific American*, March 1995, pp. 40 – 48.

[2] Barrett, D. S., et al., "Drag reduction in fish-like locomotion", *J. Fluid Mechanics*, vol. 392, Cambridge University Press, 1999, pp. 183-212.

[3] http://www.me.berkeley.edu/hel/calibot.htm

[4] http://www.nmri.go.jp/eng/khirata/fish/index_e.html

[5] Anderson, J.M. and Kerrebrock, P.A., "The Vorticity Control Unmanned Undersea Vehicle (VCUUV) Performance Results," *Proc. 11th Int. Symp. on Unmanned Untethered Submersible Technology*, Durham, NH, August 1999. Also, Draper Report no. P-3747.

[6] Triantafyllou, G. S., et al., "Optimal Thrust Development In Oscillating Foils With Application To Fish Swimming", *J. of Fluids and Structures*, Vol. 7, No. 2, February 1993, pp. 205-224.

[7] Gray J., "Studies in animal locomotion VI: The propulsive powers of the dolphin", *Journal Expl. Biol.*, 13, 1936, pp. 192-199.

[8] Ayers J., Wilbur C., and Olcott C., "Lamprey Robots", *Proceedings of the International Symposium on Aqua Biomechanisms*, Tokai University, 2000.

[9] Hollerbach J., et al., "A Comparative Analysis of Actuator Technologies for Robotics", *Robotics Review 2*, MIT Press, Cambridge MA, 1991.

[10] Newman, J. N., *Marine Hydrodynamics*, MIT Press, Cambridge, Massachusetts, 1977.

[11] White F., *Fluid mechanics*, Third Edition, McGraw Hill International Editions, 1994.